This is a pre print version of the following article:

Unveiling the nature of electronic transitions in RbV3Sb5 with avoided level crossing μSR / Bonfà, Pietro; Pratt, Francis; Valenti, Diego; Onuorah, Ifeanyi John; Kataria, Anshu; Baker, Peter J.; Cottrell, Stephen; Salinas, Andrea Capa; Wilson, Stephen D.; Guguchia, Zurab; Sanna, Samuele. - In: PHYSICAL REVIEW RESEARCH. - ISSN 2643-1564. - 7:3(2025), pp. 1-8. [10.1103/bvgk-q2qn]

Terms of use:

The terms and conditions for the reuse of this version of the manuscript are specified in the publishing policy. For all terms of use and more information see the publisher's website.

16/05/2026 17:35

(Article begins on next page)

Letter

Unveiling the nature of electronic transitions in RbV_3Sb_5 with avoided level crossing μSR

Pietro Bonfà,[1,2,*] Francis Pratt,[3] Diego Valenti,[4] Ifeanyi John Onuorah,[4] Anshu Kataria,[4] Peter J. Baker,[3] Stephen Cottrell,[3] Andrea Capa Salinas,[5] Stephen D. Wilson,[5] Zurab Guguchia,[6,†] and Samuele Sanna[7]

[1]*Dipartimento di Fisica, Informatica e Matematica, Università di Modena e Reggio Emilia, Via Campi 213/a, I-41125 Modena, Italy*

[2]*CNR-NANO S3—Istituto Nanoscienze, I-41125 Modena, Italy*

[3]*ISIS Pulsed Neutron and Muon Source, Rutherford Appleton Laboratory, Didcot OX11 0QX, United Kingdom*

[4]*Dipartimento di Scienze Matematiche, Fisiche e Informatiche, Università di Parma, I-43124 Parma, Italy*

[5]*Materials Department, University of California Santa Barbara, Santa Barbara, California 93106, USA*

[6]*PSI Center for Neutron and Muon Sciences CNM, 5232 Villigen PSI, Switzerland*

[7]*Dipartimento di Fisica e Astronomia "A. Righi", Università di Bologna, I-40127 Bologna, Italy*

(Received 19 November 2024; accepted 23 July 2025; published 2 September 2025)

Layered kagome metals AV_3Sb_5 provide a unique platform for studying the interplay between a variety of electronic orders, including superconductivity, charge density waves, nematic phases, and more. Understanding the evolution of the electronic state from the charge density wave to the superconducting transition is essential for unraveling the interplay of charge, spin, and lattice degrees of freedom giving rise to the unusual magnetic properties of these nonmagnetic metals. Previous zero-field and high-field muon spin relaxation (μSR) studies revealed two anomalies in the muon spin relaxation rate, a first change at $T_{CDW} \sim 100$ K and a second steep increase at $T^* \sim 40$ K, further enhanced by an applied magnetic field, thus suggesting a contribution of magnetic origin. In this Letter, we use the avoided level crossing μSR technique to investigate charge order in near-zero applied field. By tracking the temperature dependence of quadrupolar level-crossing resonances, we examined the evolution of the electric field gradient at V nuclei in the kagome plane. Our results show a significant rearrangement of the charge density starting at T^* indicating a transition in the charge distribution, likely electronic in origin, well below T_{CDW}. These findings, combined with previous μSR, scanning tunneling microscopy, and nuclear magnetic resonance (NMR) studies, emphasize the intertwined nature of proximate phases in these systems, with the charge rearrangement dominating the additional increase in μSR relaxation rate below T^*.

DOI: 10.1103/bvgk-q2qn

Introduction. Transition-metal-based kagome materials AV_3Sb_5 (A = K, Rb, Cs) have generated increasing interest in the scientific community owing to the diverse physical properties that have been observed, including nontrivial band topology, anomalous Hall effect [1], and an intriguing interplay between superconductivity and unconventional charge density wave (CDW) [2,3]. Despite numerous theoretical and experimental investigations, even when focusing only on the normal state, the current understanding of the cascade of transitions characterizing the electronic behavior of these compounds remains incomplete. Initially, with decreasing temperature, a CDW transition occurs at $T_{CDW} \sim 78$–102 K depending on the alkali metal [4]. In this phase, the hexagonal lattice with $P6/mmm$ symmetry undergoes a distortion involving the formation of V hexamers and trimers, which produces the so-called trihexagonal structure (TrH) in the kagome planes with the crystal adopting the $Fmmm$, $Cmmm$, or $C2/m$ space group symmetry [5–11]. This phase also features an additional modulation along the c axis, likely due to a staggered displacement pattern of the kagome layers, although some uncertainty on the mutual arrangement of these planes persists [5,12–15], probably owing to the delicate competition between CDW orders with different stacking modulations [16]. At lower temperature, the presence of a nematic transition breaking the C_6 symmetry of the kagome planes [17] has been first supported by scanning tunneling microscopy (STM) and nuclear magnetic resonance for CsV_3Sb_5 and KV_3Sb_5 [18–20], but its nature (and existence) is still debated in the literature [3,21–25]. In the bulk, this and other symmetry-breaking charge order instabilities were only identified in CsV_3Sb_5 [19,26], while no other charge order transitions between T_{CDW} and T_{SC} have been reported for A = K, Rb.

A distinctive feature of kagome systems is the potential for time-reversal symmetry (TRS) breaking in the normal state, as initially suggested by high-field scanning tunneling microscopy [27], along with evidence from a combination of zero-field and high-field muon spin relaxation (μSR) [28], supported by various experiments [29–32], such as magnetochiral anisotropy, the anomalous Hall effect [1], and

*Contact author: pietro.bonfa@posteo.net
†Contact author: zurab.guguchia@psi.ch

Published by the American Physical Society under the terms of the Creative Commons Attribution 4.0 International license. Further distribution of this work must maintain attribution to the author(s) and the published article's title, journal citation, and DOI.

magneto-optical Kerr effect (MOKE) measurements [33]. Several theoretical studies [34–42] attribute the TRS-breaking signal to orbital current phases. Furthermore, polarized neutron diffraction experiments hint at the presence of a weak magnetic signal in the second Brillouin zone at $M_2 = (1/2, 1/2, 0)$ [43]. This finding, interpreted as loop current patterns localized on vanadium triangles, reports an ordered orbital magnetic moment of at most $0.02\mu_B$ per vanadium triangle. However, whether the system breaks TRS spontaneously, i.e., in zero applied magnetic field, has been challenged by MOKE [44–46] studies that have reported no observable Kerr response in zero field (ZF). A recent analysis of transport properties suggests that the origin of the controversial reports is an extraordinary sensitivity to weak perturbations, in particular strain and magnetic fields [47]. This is in line with earlier high-field μSR experiments revealing a significant enhancement of muon relaxation rates with out-of-plane magnetic fields and with high-field STM experiments, which showed CDW intensity switching under out-of-plane magnetic fields and in-plane electric fields, implying an unusual piezomagnetic response [31].

ZF-μSR is one of the cleanest methods to identify TRS breaking owing to the possibility of performing ZF experiments on bulk samples and thanks to its sensitivity to extremely small magnetic fields [48]. For this reason, a large number of experiments have been conducted [26,28,49–53]. Previous ZF-μSR studies [26,52] on RbV_3Sb_5 have revealed a two-step increase in the relaxation rate, a smaller one at $T_{CDW} \simeq 100\,\mathrm{K}$ and a second one at $T^* \lesssim 50\,\mathrm{K}$. The increase in the relaxation rate corresponds to internal fields on the order of 0.01 mT. The effect is enhanced under an applied magnetic field, thus suggesting a magnetic contribution to the relaxation. A significant enhancement of the relaxation is also detected near the surface region of RbV_3Sb_5, specifically within 30 nm from the surface [54]. A similar two-step increase in the relaxation rate was observed in the sister compound CsV_3Sb_5, at $T_{CDW} \simeq 90\,\mathrm{K}$ and at $T^* \simeq 30\,\mathrm{K}$ [50,51]. However, the nature of the additional increase in the relaxation rate below T^* remains uncertain, leaving open the question of whether this increase is magnetic in origin or whether changes in the charge order also contribute.

In this Letter, we report the experimental results obtained with avoided level crossing (ALC) μSR, which enables the study of charge distribution evolution by monitoring changes in the electric field gradient (EFG) tensor at nuclei with spin $I > 1/2$, located near the muon. This information is obtained indirectly through the dipolar coupling between the muon and quadrupole-active nuclei. By finely tuning the muon Zeeman energy to match a nuclear quadrupolar splitting, a cross relaxation between the spins known as muon quadrupole level crossing resonance (μ-QLCR or simply QLCR) takes place. As a consequence, one can selectively probe different nuclei by matching different quadrupolar energies, whereas in ZF experiments the nuclear contribution to the polarization function is dominated by the dipolar interaction between the muon and the nearest nuclei. A nice review of this approach is presented in Ref. [55]. The μSR-based approach for collecting quadrupolar splittings has proven to be especially valuable in scenarios where the signal in conventional nuclear quadrupole resonance (NQR) experiments is weak, hidden by other resonances, or technically challenging to collect. This applies indeed to the case of AV_3Sb_5, as ^{51}V NQR is difficult to perform owing to its low frequency and the strongest antimony NQR signal is due to the interlayer graphenelike sheets, while the more interesting in-plane Sb resonances are very weak [8,56]. This, and the fact that the muon happens to stop close to the kagome plane [54] giving us good sensitivity for probing the V atoms, represents the main motivation behind the strategy adopted in this work.

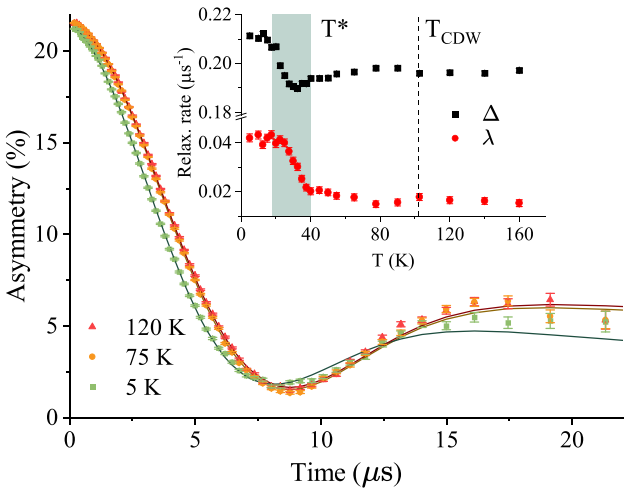

FIG. 1. The ZF-μSR spectra of RbV_3Sb_5. The main panel depicts three high-statistics acquisitions showing the evolution of the asymmetry as a function of the temperature. A tiny difference is observed between signals above (120 K) and below (75 K) the CDW transition (102 K). A noticeably faster relaxation is instead observed in the measurement performed at 5 K. The continuous lines are best fits to Eq. (1). The inset shows the temperature evolution of the fitting parameters resulting from the analysis described in the main text.

Results. For all experiments, we used finely ground RbV_3Sb_5 powders, identical to the sample in Ref. [54]. Both the ZF and the ALC acquisitions have been carried out using the EMU spectrometer [57] at the ISIS pulsed muon facility. The ZF-μSR data are shown in Fig. 1. The asymmetry has been analyzed with best fits to the equation

$$A(t) = A_0\left[\tfrac{1}{3} + \tfrac{2}{3}(1-\Delta^2 t^2)e^{-\Delta^2 t^2/2}\right]e^{-\lambda t} + B \qquad (1)$$

for consistency to the previous literature [50–52]. In Eq. (1), A_0 is the relaxing asymmetry, B is a baseline, and the function in square brackets is the Kubo-Toyabe (KT) function [48] characterized by a relaxation rate Δ and multiplied by an additional Lorentzian relaxation, parameterized by λ. This phenomenological approach matches very well with the experimental data at short time, while small deviations are observed for $t > 13\,\mu\mathrm{s}$ in the $T = 75$ and 120 K measurements, as depicted in Fig. 1. A dramatic discrepancy is instead observed at 5 K for $t > 10\,\mu\mathrm{s}$, showing the limits of the phenomenological description based on Eq. (1). Notably, the tail of the 5 K signal remains relatively flat, indicating a lack of dynamic effects. It should be noted that the KT function in Eq. (1) arises from a semiclassical description of the muon-nuclei interaction. For this reason, an additional relaxation contribution and a (temperature-dependent) baseline B are required. Departures from the semiclassical prediction

are common and are generally found in the long-time tail, as shown, for example, in Ref. [58], though relevant effects can also take place at shorter times [59,60]. A very accurate prediction of the ZF muon polarization function above T^* can be obtained from first-principles modeling of the muon site and its interaction with the neighboring nuclei, when the entire description is performed at the quantum mechanical level. These results, already presented in Ref. [54] together with a detailed description of the muon sites, reveal that the ZF signal is most sensitive to the in-plane Sb atoms through a simple dipolar interaction between the muon spin and the nearest-neighboring Sb isotopes ($m_{^{121}\mathrm{Sb}} = 3.36\mu_P$, $m_{^{123}\mathrm{Sb}} = 2.55\mu_P$, and $d_{\mu\text{-Sb}} \sim 1.7$ Å), while the coupling with the V nuclei forming the kagome lattice is much weaker ($m_{^{51}V} = 5.15\mu_P$ and $d_{\mu\text{-}V} \sim 3.5$ Å). However, in the following discussion, we still opt for the phenomenological model due to its simplicity and effectiveness in capturing the transitions observed in the ZF data.

The inset of Fig. 1 reports the temperature evolution of λ and Δ obtained from best fits of the measurements performed in the temperature interval 5–160 K. Two transitions can be detected, at about $T_{\mathrm{CDW}} = 100$ K and $T^* = 40$ K. The trend follows what has been already reported in the literature [52]. As can be appreciated from the main panel of Fig. 1, the transition at T_{CDW} has a small effect on the polarization function of the muon. This can be easily rationalized: V atoms, which undergo the largest displacements at T_{CDW}, are also the most weakly coupled with the muon. On the other hand, a marked change takes place below T^* as shown also by the difference between the raw data acquired at 5 and 75 K (Fig. 1, main panel). The extended time window of our new measurements provides a more detailed picture of the evolution of the μSR signal as a function of the temperature. From the phenomenological analysis, considering both λ and Δ, the broad transition that starts at $T^* = 40$ K is finally completed at $T \sim 20$ K, where both the relaxation coefficients become temperature independent.

Longitudinal field ALC experiments have been performed with $\mu_0 H$ ranging from 2.3 to 13.1 mT. In order to reduce the noise of the data, we employ a field-differential approach [61], where the external magnetic field is varied by ± 0.2 mT during the acquisition, thus removing the instabilities of the beam affecting the raw data. The resulting time-integrated (TI) field-differential signal is numerically integrated to produce the curves $I(x)$ reported in Fig. 2, which clearly show a large temperature dependence (see the Supplemental Material [62] for details). These results are fitted to the equation

$$I(x) = I_0\left(1 - \frac{\tau}{x^N}\right) - \sum_{i=1}^{2} \frac{A_i}{\sigma_i\sqrt{2\pi}} \exp\left(-\frac{1}{2}\frac{\left(x - B_i^{\mathrm{res}}\right)^2}{\sigma_i^2}\right) \tag{2}$$

for $x = \mu_0 H$ in the range 2.4–13.1 mT. In Eq. (2), I_0 is the value of the integrated asymmetry for $x \to \infty$. The first term on the right-hand side is used to phenomenologically approximate the TI polarization function of pure dipolar origin in longitudinal applied field conditions and in the absence of resonances, and the two parameters τ and N are used to extract its field dependence, which is considered the background in our measurements. The chosen expression

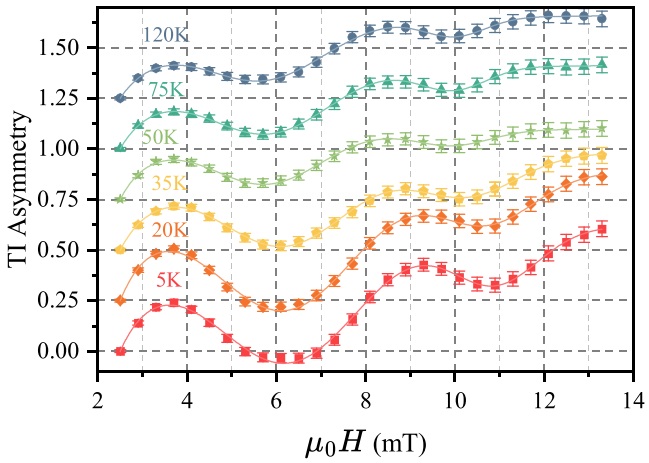

FIG. 2. ALC results and analysis as a function of temperature. The points show the numerical integration of the TI field-differential acquisitions. The continuous lines are best fit to the data according to Eq. (2) described in the main text.

aims at reducing the number of free parameters in our fits, while we use a combination of linear, quadratic, and cubic terms to extract the background term in a second set of fits described in the following section. The observed level-crossing resonances are instead captured by the second term of Eq. (2) with two Gaussian functions, each characterized by three parameters: A, B^{res}, and σ, respectively, the area, the resonance field, and the width of the resonance. The results of the fit are shown in Fig. 3. Surprisingly, the CDW transition has a very slight effect, if any, on the resonance parameters, while sizable deviations are observed for $T \lesssim T^*$. Indeed, the area of both resonances, shown in Fig. 3(a), increases below 40 K and it remains constant between 20 and 5 K. The resonant fields, shown in Fig. 3(b), also display a clear shift on the order of 1 mT when the temperature drops below 40 K. Finally, a similar temperature dependence is also observed for the width of the resonance peaks in Fig. 3(c), although the actual trend for the second resonance is impaired by the large uncertainty of this parameter.

Microscopic analysis of ALC. In order to understand the microscopic origin of the ALC resonances, we exploit the *ab initio* density functional theory (DFT) results already published in Refs. [54,63] and [8,64]. In the former, the muon site and the perturbation induced on the lattice by the muon are predicted for RbV_3Sb_5 using a plane-wave (PW) basis. From the latter, we collect more accurate full-potential augmented plane wave (APW)-based estimations of the EFGs at nuclear sites (further details are provided in Ref. [62]). PW-based results provide valuable information toward the identification of the nuclei involved in a QLCR producing the experimental signal. It is found indeed that, for the field range of the measurement, a hexagon of six V atoms close to the muon site contributes most significantly to the QLCR spectra, while the remaining nuclei produce resonances at smaller (Rb) or larger (Sb) fields (see Ref. [62]). This allows us to proceed considering only V atoms and switching to full-potential simulation results in light of the small perturbation introduced by the muon on the vanadium sublattice [65]. In the TrH

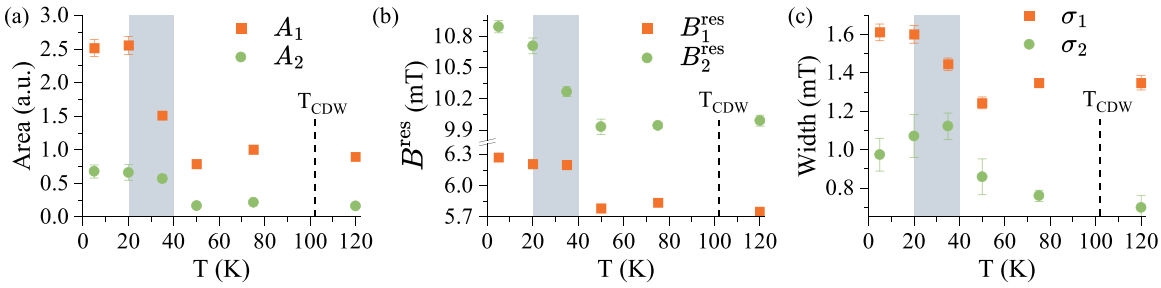

FIG. 3. Parameters obtained from best-fit curves shown in Fig. 2. Panel (a) shows the area of the Gaussian used to describe the two resonances, panel (b) shows the resonant field, and panel (c) shows the width of the two Gaussian functions. The gray shading shows the same temperature interval displayed in Fig. 1, where the second low-temperature transition takes place according to ZF results.

structure, there are only two symmetrically distinct muon sites and we compute, for each of them, the polarization function arising from the interaction between the muon and six NN V atoms, using the method introduced by Celio [66,67]. To check for convergence of our simulations, we also include the NN Sb atom (the ^{121}Sb isotope is only considered). The nuclear quadrupolar coupling constant C_Q, defined as

$$C_Q = \frac{e_0 V_{zz} Q}{h}, \tag{3}$$

where $Q = -0.043(5)$ barn is the quadrupolar moment of ^{51}V [68] and V_{zz} is the largest eigenvalue of the EFG tensor, is predicted, from APW simulations, to be $C_Q^{\mathrm{APW}} = 7$ MHz, and the asymmetry parameter $\eta = (V_{xx} - Vyy)/V_{zz}$ is $\eta^{\mathrm{APW}} = 0.43$. The inclusion of the NN Sb in the Hilbert space negligibly affects the resonances and only alters the TI asymmetry for $B \to 0$ (not shown) [69]. The resulting curves, shown in Fig. 4(a), match very well with the experimental results above T^*. In addition, by comparison with the ones obtained in the high-temperature hexagonal phase, they confirm that this probe is almost insensitive to the CDW order: The two signals only differ by some broadening and the only noticeable change is at about 11 mT.

Unfortunately, this approach is computationally demanding and prevents fitting the microscopic QLCR parameters C_Q and η to the experimental data. Therefore, since the muon is close to the center of the hexagon and the magnitudes of the EFG parameters are similar for all six, for fitting purposes we took one V site as representative and calculated the polycrystalline averaged QLCR spectrum versus η with the principal axis of the field gradient aligned at 90° to the muon vector. The QLCR for the six V sites was then evaluated by scaling the resonance amplitude by a factor of 6. Finally, a cubic polynomial is added to account for the background due to minor contributions from other nuclei. This approach yields an average trend and assumes that the dipolar interactions between V nuclei are not significant compared to the dipolar interaction between the muon and each individual V. This model requires a reduced Hilbert space (consisting of the muon and one V atom at a time), allowing us to extract an averaged trend for the parameters describing the dipolar and quadrupolar coupling of the V nuclei with the muon and the surrounding electronic charge, respectively. We fit the TI asymmetry (shown in Ref. [62]) and report the results in Fig. 4. The amplitude A quantifies the ratio between the predicted depth of the resonances and the experimentally observed ones.

Discussion. With the microscopic origin of the QLCR clarified, we now turn our attention to the temperature evolution of the ALC measurement and its relationship with previous ZF measurements. The results of the two approaches, summarized by the plots of Fig. 4, show that a very nice agreement between the experiments and first-principles calculations [8] in the high-temperature phase can also be obtained for ALC-μSR measurements. The values for C_Q and η that can be extracted from the ALC data match well with previous NMR results [8,14] and with APW-based estimates. The microscopic picture also allows to explain why ALC-μSR is also

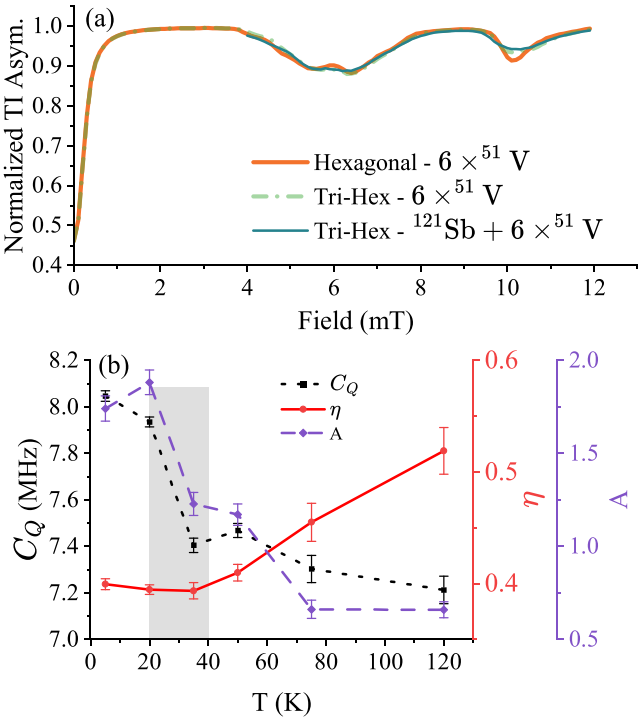

FIG. 4. (a) Predicted resonances for $T > T_{\mathrm{CDW}}$ in the hexagonal structure and for the low-temperate TrH structure (neglecting the modulation along the c axis). The legend also reports the cluster of nuclei included in the simulation. The EFGs at V and Sb sites are obtained from a full-potential DFT-based prediction. (b) Results of the fit of TI asymmetry to the microscopic model described in the main text.

almost insensitive to the CDW transition. At the transition, the EFG at V nuclei varies very little [70] and the two V sublattices that appear in the TrH phase have the same multiplicity and slightly decreasing or increasing V_{zz} with respect to their common value above the CDW transition (see Refs. [8,62]), resulting only in a small broadening of the QLCRs.

The phenomenological and the microscopic analysis, shown in Figs. 3 and 4(b), respectively, shows roughly the same temperature trend for $B^{\rm res}$ and C_Q ($B^{\rm res}$ depends on both C_Q and η) and for the depth of the resonance, the parameter A. They all display a sharp increase as temperature decreases below about 40 K. Interestingly, the resulting variation of V_{zz} at V nuclei probed by muons, on the order of 5%, is slightly larger than the one reported by high-field NMR measurements in CsV_3Sb_5 (see the Supplemental Material of Ref. [21]). Remarkably, the ZF muon spin relaxation rates Δ and λ (inset of Fig. 1), the phenomenological ALC parameters A_i, B_i, and σ_i (Fig. 3), and the results of the microscopic model [Fig. 4(b)] exhibit similar temperature dependence, as highlighted by the shaded region. A key question is whether the ALC resonance field shift, shown in Fig. 3(b), can be attributed to an additional field generated by weak magnetic interactions. The ZF relaxation rate increasing by $\delta\lambda \lesssim 0.03\ \mu s^{-1}$ corresponds to a local field increase of $\delta B = \delta\lambda/(\gamma_\mu) \sim 0.035\,\text{mT}$ [71]. However, the observed shift in ALC resonance is more than an order of magnitude larger. Therefore, the contribution to the increase of ALC resonance field from magnetic coupling between the muon and the electronic channel via orbital or spin magnetism is minimal. We conclude that the increase of the resonant field is primarily due to a shift in nuclear quadrupolar energy levels, caused by charge redistribution at the V sites, indicating the presence of a transition in the charge channel setting in before the onset of superconductivity.

The key question now is what drives this charge redistribution. Given the lack of thermodynamic evidence for a transition at $T^* \sim 40\,\text{K}$ and the absence of major structural distortions, this cannot be attributed to simple structural changes. Notably, NMR experiments and STM measurements in CsV_3Sb_5 and KV_3Sb_5 [19,21,23,72] have reported additional charge density wave instabilities and rotational symmetry broken states stabilized well below the CDW order. It is plausible to assume that the charge redistribution observed below $T^* \sim 40\,\text{K}$ in RbV_3Sb_5 shares a similar origin with CsV_3Sb_5 hinting at electronic nematicity.

Conclusions. We have presented ZF-μSR and ALC-μSR experiments performed on RbV_3Sb_5. With the latter technique, we investigated the evolution of charge order in the kagome plane. Our results reveal a significant rearrangement of charge density around the muon below $T^* \sim 40\,\text{K}$, an effect that matches with the upturn of the muon relaxation rate observed in ZF-μSR. This uncovers a hitherto unnoticed charge order transition in RbV_3Sb_5 well below the onset of the CDW and before the system enters the superconducting state, showing that a nontrivial evolution of the local charge and electronic landscape is the primary origin for the phenomenology observed in zero and near-zero field conditions below T^*. These findings, combined with previous high-field μSR, NMR, STM, and transport studies, demonstrate that the charge and spin channels are strongly intertwined in these materials.

Furthermore, this study highlights the effectiveness of ALC-μSR measurements as a powerful tool for probing electronic orders. Additional experimental and computational investigations, potentially utilizing resonances of other quadrupolar nuclei (Rb, Sn, Cs, K), will be essential to further elucidate the microscopic long-range order below T^* in this and related compounds.

Acknowledgments. We thank Roberto De Renzi and Giuseppe Allodi for insightful discussions. The computational resources were provided by the SCARF cluster of the STFC Scientific Computing Department and by the ISCRA initiative of CINECA with project IsCb6_TRSBKS. Work in Parma was funded by the PNRR MUR Project No. ECS-00000033-ECOSISTER. I.J.O. acknowledges support by the University of Parma through the action Bando di Ateneo 2023 per la ricerca. S.D.W. and A.C.S. gratefully acknowledge support via the UC Santa Barbara NSF Quantum Foundry funded via the Q-AMASE-i program under award DMR-1906325. Z.G. acknowledges support from the Swiss National Science Foundation (SNSF) through SNSF Starting (Grant No. TMSGI2_211750).

Data availability. The data supporting this article are openly available from the Materials Cloud Archives [63,64] and from the ISIS Data Gateway [86].

[1] S.-Y. Yang, Y. Wang, B. R. Ortiz, D. Liu, J. Gayles, E. Derunova, R. Gonzalez-Hernandez, L. Šmejkal, Y. Chen, S. S. P. Parkin, S. D. Wilson, E. S. Toberer, T. McQueen, and M. N. Ali, Giant, unconventional anomalous Hall effect in the metallic frustrated magnet candidate, KV_3Sb_5, Sci. Adv. **6**, eabb6003 (2020).

[2] T. Neupert, M. M. Denner, J.-X. Yin, R. Thomale, and M. Z. Hasan, Charge order and superconductivity in kagome materials, Nat. Phys. **18**, 137 (2022).

[3] M. Frachet, L. Wang, W. Xia, Y. Guo, M. He, N. Maraytta, R. Heid, A.-A. Haghighirad, M. Merz, C. Meingast, and F. Hardy, Colossal c-axis response and lack of rotational symmetry breaking within the kagome planes of the CsV_3Sb_5 superconductor, Phys. Rev. Lett. **132**, 186001 (2024).

[4] M. Wenzel, B. R. Ortiz, S. D. Wilson, M. Dressel, A. A. Tsirlin, and E. Uykur, Optical study of RbV_3Sb_5: Multiple density-wave gaps and phonon anomalies, Phys. Rev. B **105**, 245123 (2022).

[5] H. Li, T. T. Zhang, T. Yilmaz, Y. Y. Pai, C. E. Marvinney, A. Said, Q. W. Yin, C. S. Gong, Z. J. Tu, E. Vescovo, C. S. Nelson, R. G. Moore, S. Murakami, H. C. Lei, H. N. Lee, B. J. Lawrie, and H. Miao, Observation of unconventional charge density wave without acoustic phonon anomaly in kagome superconductors AV_3Sb_5 (A = Rb, Cs), Phys. Rev. X **11**, 031050 (2021).

[6] A. Subedi, Hexagonal-to-base-centered-orthorhombic $4Q$ charge density wave order in kagome metals KV_3Sb_5, RbV_3Sb_5, and CsV_3Sb_5, Phys. Rev. Mater. **6**, 015001 (2022).

[7] H. Tan, Y. Liu, Z. Wang, and B. Yan, Charge density waves and electronic properties of superconducting kagome metals, Phys. Rev. Lett. **127**, 046401 (2021).

[8] J. Frassineti, P. Bonfà, G. Allodi, E. Garcia, R. Cong, B. R. Ortiz, S. D. Wilson, R. De Renzi, V. F. Mitrović, and S. Sanna, Microscopic nature of the charge-density wave in the kagome superconductor RbV_3Sb_5, Phys. Rev. Res. **5**, L012017 (2023).

[9] L. Kautzsch, B. R. Ortiz, K. Mallayya, J. Plumb, G. Pokharel, J. P. C. Ruff, Z. Islam, E.-A. Kim, R. Seshadri, and S. D. Wilson, Structural evolution of the kagome superconductors AV_3Sb_5 (A = K, Rb, and Cs) through charge density wave order, Phys. Rev. Mater. **7**, 024806 (2023).

[10] A. Ptok, A. Kobiałka, M. Sternik, J. Łażewski, P. T. Jochym, A. M. Oleś, and P. Piekarz, Dynamical study of the origin of the charge density wave in AV_3Sb_5 (A = K, Rb, Cs) compounds, Phys. Rev. B **105**, 235134 (2022).

[11] Q. Deng, H. Tan, B. R. Ortiz, S. D. Wilson, B. Yan, and L. Wu, Revealing rotational symmetry breaking charge density wave order in the kagome superconductor (Rb, K)V_3Sb_5 by ultrafast pump-probe experiments, Phys. Rev. B **111**, 165134 (2025).

[12] B. R. Ortiz, S. M. L. Teicher, L. Kautzsch, P. M. Sarte, N. Ratcliff, J. Harter, J. P. C. Ruff, R. Seshadri, and S. D. Wilson, Fermi surface mapping and the nature of charge-density-wave order in the kagome superconductor CsV_3Sb_5, Phys. Rev. X **11**, 041030 (2021).

[13] Q. Stahl, D. Chen, T. Ritschel, C. Shekhar, E. Sadrollahi, M. C. Rahn, O. Ivashko, M. v. Zimmermann, C. Felser, and J. Geck, Temperature-driven reorganization of electronic order in CsV_3Sb_5, Phys. Rev. B **105**, 195136 (2022).

[14] X. Zhang, Y. Li, J. Zheng, F. Zhou, Q. Wu, X. Xi, Y. Lau, Z. Wang, and W. Wang, NMR study of charge density wave phase in the kagome metal RbV_3Sb_5, Appl. Phys. Lett. **124**, 093106 (2024).

[15] V. Scagnoli, L. J. Riddiford, S. W. Huang, Y.-G. Shi, Z. Tu, H. Lei, A. Bombardi, G. Nisbet, and Z. Guguchia, Resonant x-ray diffraction measurements in charge ordered kagome superconductors KV_3Sb_5 and RbV_3Sb_5, J. Phys.: Condens. Matter **36**, 185604 (2024).

[16] C. Park and Y.-W. Son, Condensation of preformed charge density waves in kagome metals, Nat. Commun. **14**, 7309 (2023).

[17] It should be noted that, while at T_{CDW} the rotational symmetry of the system changes from C_6 to C_2 owing to the staggered order along c, the kagome layers retain the original sixfold rotational symmetry. Yet, at lower temperature, the C_6 symmetry of the 2D kagome layer may also be broken by the so-called "strong" nematic state (to distinguish it from the "weak" nematic state realized at T_{CDW} [73]).

[18] H. Zhao, H. Li, B. R. Ortiz, S. M. L. Teicher, T. Park, M. Ye, Z. Wang, L. Balents, S. D. Wilson, and I. Zeljkovic, Cascade of correlated electron states in the kagome superconductor CsV_3Sb_5, Nature (London) **599**, 216 (2021).

[19] J. Luo, Z. Zhao, Y. Z. Zhou, J. Yang, A. F. Fang, H. T. Yang, H. J. Gao, R. Zhou, and G.-Q. Zheng, Possible star-of-David pattern charge density wave with additional modulation in the kagome superconductor CsV_3Sb_5, npj Quantum Mater. **7**, 30 (2022).

[20] H. Li, H. Zhao, B. R. Ortiz, T. Park, M. Ye, L. Balents, Z. Wang, S. D. Wilson, and I. Zeljkovic, Rotation symmetry breaking in the normal state of a kagome superconductor KV_3Sb_5, Nat. Phys. **18**, 265 (2022).

[21] L. Nie, K. Sun, W. Ma, D. Song, L. Zheng, Z. Liang, P. Wu, F. Yu, J. Li, M. Shan, D. Zhao, S. Li, B. Kang, Z. Wu, Y. Zhou, K. Liu, Z. Xiang, J. Ying, Z. Wang, and T. Wu *et al.*, Charge-density-wave-driven electronic nematicity in a kagome superconductor, Nature (London) **604**, 59 (2022).

[22] Y. Sur, K.-T. Kim, S. Kim, and K. H. Kim, Optimized superconductivity in the vicinity of a nematic quantum critical point in the kagome superconductor $Cs(V_{1-x}Ti_x)_3Sb_5$, Nat. Commun. **14**, 3899 (2023).

[23] H. Li, H. Zhao, B. R. Ortiz, Y. Oey, Z. Wang, S. D. Wilson, and I. Zeljkovic, Unidirectional coherent quasiparticles in the high-temperature rotational symmetry broken phase of AV_3Sb_5 kagome superconductors, Nat. Phys. **19**, 637 (2023).

[24] Z. Liu, Y. Shi, Q. Jiang, E. W. Rosenberg, J. M. DeStefano, J. Liu, C. Hu, Y. Zhao, Z. Wang, Y. Yao, D. Graf, P. Dai, J. Yang, X. Xu, and J.-H. Chu, Absence of E_{2g} nematic instability and dominant A_{1g} response in the kagome metal CsV_3Sb_5, Phys. Rev. X **14**, 031015 (2024).

[25] T. Asaba, A. Onishi, Y. Kageyama, T. Kiyosue, K. Ohtsuka, S. Suetsugu, Y. Kohsaka, T. Gaggl, Y. Kasahara, H. Murayama, K. Hashimoto, R. Tazai, H. Kontani, B. R. Ortiz, S. D. Wilson, Q. Li, H. H. Wen, T. Shibauchi, and Y. Matsuda, Evidence for an odd-parity nematic phase above the charge-density-wave transition in a kagome metal, Nat. Phys. **20**, 40 (2024).

[26] S. D. Wilson and B. R. Ortiz, AV_3Sb_5 kagome superconductors, Nat. Rev. Mater. **9**, 420 (2024).

[27] Y.-X. Jiang, J.-X. Yin, M. M. Denner, N. Shumiya, B. R. Ortiz, G. Xu, Z. Guguchia, J. He, M. S. Hossain, X. Liu, J. Ruff, L. Kautzsch, S. S. Zhang, G. Chang, I. Belopolski, Q. Zhang, T. A. Cochran, D. Multer, M. Litskevich, and Z.-J. Cheng *et al.*, Unconventional chiral charge order in kagome superconductor KV_3Sb_5, Nat. Mater. **20**, 1353 (2021).

[28] C. Mielke, D. Das, J.-X. Yin, H. Liu, R. Gupta, Y.-X. Jiang, M. Medarde, X. Wu, H. C. Lei, J. Chang, P. Dai, Q. Si, H. Miao, R. Thomale, T. Neupert, Y. Shi, R. Khasanov, M. Z. Hasan, H. Luetkens, and Z. Guguchia, Time-reversal symmetry-breaking charge order in a kagome superconductor, Nature (London) **602**, 245 (2022).

[29] D. Chen, B. He, M. Yao, Y. Pan, H. Lin, W. Schnelle, Y. Sun, J. Gooth, L. Taillefer, and C. Felser, Anomalous thermoelectric effects and quantum oscillations in the kagome metal CsV_3Sb_5, Phys. Rev. B **105**, L201109 (2022).

[30] C. Guo, C. Putzke, S. Konyzheva, X. Huang, M. Gutierrez-Amigo, I. Errea, D. Chen, M. G. Vergniory, C. Felser, M. H. Fischer, T. Neupert, and P. J. W. Moll, Switchable chiral transport in charge-ordered kagome metal CsV_3Sb_5, Nature (London) **611**, 461 (2022).

[31] Y. Xing, S. Bae, E. Ritz, F. Yang, T. Birol, A. N. Capa Salinas, B. R. Ortiz, S. D. Wilson, Z. Wang, R. M. Fernandes, and V. Madhavan, Optical manipulation of the charge-density-wave state in RbV_3Sb_5, Nature (London) **631**, 60 (2024).

[32] H. Deng, G. Liu, Z. Guguchia, T. Yang, J. Liu, Z. Wang, Y. Xie, S. Shao, H. Ma, W. Liège, F. Bourdarot, X.-Y. Yan, H. Qin, C. Mielke III, R. Khasanov, H. Luetkens, X. Wu, G. Chang, J. Liu, M. H. Christensen *et al.*, Evidence for time-reversal symmetry-breaking kagome superconductivity, Nat. Mater. **23**, 1639 (2024).

[33] Y. Xu, Z. Ni, Y. Liu, B. R. Ortiz, Q. Deng, S. D. Wilson, B. Yan, L. Balents, and L. Wu, Three-state nematic-

ity and magneto-optical Kerr effect in the charge density waves in kagome superconductors, Nat. Phys. **18**, 1470 (2022).

[34] Y.-P. Lin and R. M. Nandkishore, Complex charge density waves at Van Hove singularity on hexagonal lattices: Haldane-model phase diagram and potential realization in the kagome metals AV_3Sb_5 (A = K, Rb, Cs), Phys. Rev. B **104**, 045122 (2021).

[35] T. Park, M. Ye, and L. Balents, Electronic instabilities of kagome metals: Saddle points and Landau theory, Phys. Rev. B **104**, 035142 (2021).

[36] X. Feng, Y. Zhang, K. Jiang, and J. Hu, Low-energy effective theory and symmetry classification of flux phases on the kagome lattice, Phys. Rev. B **104**, 165136 (2021).

[37] M. M. Denner, R. Thomale, and T. Neupert, Analysis of charge order in the kagome metal AV_3Sb_5 (A = Rb,Cs), Phys. Rev. Lett. **127**, 217601 (2021).

[38] M. H. Christensen, T. Birol, B. M. Andersen, and R. M. Fernandes, Loop currents in AV_3Sb_5 kagome metals: Multipolar and toroidal magnetic orders, Phys. Rev. B **106**, 144504 (2022).

[39] H. Li, Y. B. Kim, and H.-Y. Kee, Intertwined van Hove singularities as a mechanism for loop current order in kagome metals, Phys. Rev. Lett. **132**, 146501 (2024).

[40] K. Shimura, R. Tazai, Y. Yamakawa, S. Onari, and H. Kontani, Real-space loop current pattern in time-reversal-symmetry breaking phase in kagome metals, J. Phys. Soc. Jpn. **93**, 033704 (2024).

[41] J.-W. Dong, Z. Wang, and S. Zhou, Loop-current charge density wave driven by long-range Coulomb repulsion on the kagomé lattice, Phys. Rev. B **107**, 045127 (2023).

[42] R. Tazai, Y. Yamakawa, and H. Kontani, Charge-loop current order and Z_3 nematicity mediated by bond order fluctuations in kagome metals, Nat. Commun. **14**, 7845 (2023).

[43] W. Liège, Y. Xie, D. Bounoua, Y. Sidis, F. Bourdarot, Y. Li, Z. Wang, J.-X. Yin, P. Dai, and P. Bourges, Search for orbital magnetism in the kagome superconductor CsV_3Sb_5 using neutron diffraction, Phys. Rev. B **110**, 195109 (2024).

[44] D. R. Saykin, C. Farhang, E. D. Kountz, D. Chen, B. R. Ortiz, C. Shekhar, C. Felser, S. D. Wilson, R. Thomale, J. Xia, and A. Kapitulnik, High resolution polar kerr effect studies of CsV_3Sb_5: Tests for time-reversal symmetry breaking below the charge-order transition, Phys. Rev. Lett. **131**, 016901 (2023).

[45] J. Wang, C. Farhang, B. R. Ortiz, S. D. Wilson, and J. Xia, Resolving the discrepancy between MOKE measurements at 1550-nm wavelength on kagome metal CsV_3Sb_5, Phys. Rev. Mater. **8**, 014202 (2024).

[46] C. Farhang, J. Wang, B. R. Ortiz, S. D. Wilson, and J. Xia, Unconventional specular optical rotation in the charge ordered state of Kagome metal CsV_3Sb_5, Nat. Commun. **14**, 5326 (2023).

[47] C. Guo, G. Wagner, C. Putzke, D. Chen, K. Wang, L. Zhang, M. Gutierrez-Amigo, I. Errea, M. G. Vergniory, C. Felser, M. H. Fischer, T. Neupert, and P. J. W. Moll, Correlated order at the tipping point in the kagome metal CsV_3Sb_5, Nat. Phys. **20**, 579 (2024).

[48] S. Blundell, R. De Renzi, T. Lancaster, and F. Pratt, *Muon Spectroscopy: An Introduction* (Oxford University Press, Oxford, 2022).

[49] L. Yu, C. Wang, Y. Zhang, M. Sander, S. Ni, Z. Lu, S. Ma, Z. Wang, Z. Zhao, H. Chen, K. Jiang, Y. Zhang, H. Yang, F. Zhou, X. Dong, S. L. Johnson, M. J. Graf, J. Hu, H.-J. Gao, and Z. Zhao, Evidence of a hidden flux phase in the topological kagome metal CsV_3Sb_5, arXiv:2107.10714.

[50] Z. Shan, P. K. Biswas, S. K. Ghosh, T. Tula, A. D. Hillier, D. Adroja, S. Cottrell, G.-H. Cao, Y. Liu, X. Xu, Y. Song, H. Yuan, and M. Smidman, Muon spin relaxation study of the layered kagome superconductor CsV_3Sb_5, Phys. Rev. Res. **4**, 033145 (2022).

[51] R. Khasanov, D. Das, R. Gupta, C. Mielke, M. Elender, Q. Yin, Z. Tu, C. Gong, H. Lei, E. T. Ritz, R. M. Fernandes, T. Birol, Z. Guguchia, and H. Luetkens, Time-reversal symmetry broken by charge order in CsV_3Sb_5, Phys. Rev. Res. **4**, 023244 (2022).

[52] Z. Guguchia, C. Mielke, D. Das, R. Gupta, J.-X. Yin, H. Liu, Q. Yin, M. H. Christensen, Z. Tu, C. Gong, N. Shumiya, M. S. Hossain, T. Gamsakhurdashvili, M. Elender, P. Dai, A. Amato, Y. Shi, H. C. Lei, R. M. Fernandes, and M. Z. Hasan *et al.*, Tunable unconventional kagome superconductivity in charge ordered RbV_3Sb_5 and KV_3Sb_5, Nat. Commun. **14**, 153 (2023).

[53] E. M. Kenney, B. R. Ortiz, C. Wang, S. D. Wilson, and M. J. Graf, Absence of local moments in the kagome metal KV_3Sb_5 as determined by muon spin spectroscopy, J. Phys.: Condens. Matter **33**, 235801 (2021).

[54] J. N. Graham, C. Mielke III, D. Das, T. Morresi, V. Sazgari, A. Suter, T. Prokscha, H. Deng, R. Khasanov, S. D. Wilson, A. C. Salinas, M. M. Martins, Y. Zhong, K. Okazaki, Z. Wang, M. Z. Hasan, M. H. Fischer, T. Neupert, J. X. Yin, and S. Sanna *et al.*, Depth-dependent study of time-reversal symmetry-breaking in the kagome superconductor AV_3Sb_5, Nat. Commun. **15**, 8978 (2024).

[55] S. F. J. Cox, Detection of quadrupole interactions by muon level crossing resonance, Z. Naturforsch. A **47**, 371 (1992).

[56] Y. Wang, T. Wu, Z. Li, K. Jiang, and J. Hu, Structure of the kagome superconductor CsV_3Sb_5 in the charge density wave state, Phys. Rev. B **107**, 184106 (2023).

[57] S. Giblin, S. Cottrell, P. King, S. Tomlinson, S. Jago, L. Randall, M. Roberts, J. Norris, S. Howarth, Q. Mutamba, N. Rhodes, and F. Akeroyd, Optimising a muon spectrometer for measurements at the ISIS pulsed muon source, Nucl. Instrum. Methods Phys. Res. Sect. A **751**, 70 (2014).

[58] W. Huang, V. Pacradouni, and J. E. Sonier, Calculation of nuclear contribution to the zero-field muon spin polarization function of single crystal $La_{2-X}Sr_XCuO_4$, Phys. Procedia **30**, 129 (2012).

[59] P. Bonfà, J. Frassineti, J. M. Wilkinson, G. Prando, M. M. Isah, C. Wang, T. Spina, B. Joseph, V. F. Mitrović, R. De Renzi, S. J. Blundell, and S. Sanna, Entanglement between muon and $I > \frac{1}{2}$ nuclear spins as a probe of charge environment, Phys. Rev. Lett. **129**, 097205 (2022).

[60] J. M. Wilkinson, F. Lang, P. J. Baker, S. P. Cottrell, and S. J. Blundell, Identifying muon sites by eye in KPF_6 and KBF_4, J. Phys.: Conf. Ser. **2462**, 012007 (2023).

[61] R. Kadono, W. Higemoto, A. Koda, K. Kakuta, K. Ohishi, H. Takagiwa, T. Yokoo, and J. Akimitsu, Spin dynamics of 4*f* electrons in CeB_6 studied by muon spin relaxation, J. Phys. Soc. Jpn. **69**, 3189 (2000).

[62] See Supplemental Material at http://link.aps.org/supplemental/10.1103/bvgk-q2qn for the details of muon-induced perturbations, the simulation and fitting of ALC resonances, and the computational details, which includes Refs. [8,54–56,61,63,64,66,74–82].

[63] J. N. Graham, C. Mielke, III, D. Das, T. Morresi, V. Ardakani, A. Suter, T. Prokscha, H. Deng, R. Khasanov, S. D. Wilson, A. C. Salinas, Y. Zhong, K. Okazaki, Z. Wang, M. Z. Hasan, M. Fisher, T. Neupert, J.-X. Yin, S. Sanna, H. Luetkens, Z. Salman, P. Bonfà, and Z. Guguchia, Depth-dependent time reversal symmetry breaking response in the charge-ordered kagome material RbV_3Sb_5, Materials Cloud Archive 2024.30 (2024), https://doi.org/10.24435/materialscloud:4f-r5.

[64] J. Frassineti, P. Bonfà, G. Allodi, E. Garcia, R. Cong, B. R. Ortiz, S. D. Wilson, R. D. Renzi, V. F. Mitrović, and S. Sanna, Microscopic nature of the charge-density wave in the kagome superconductor RbV_3Sb_5, Materials Cloud Archive 2024.22 (2024), https://doi.org/10.24435/materialscloud:n0-va.

[65] At difference with the nearest-neighboring Sb and, to a lesser extent, to the second-nearest-neighboring Rb where muon-induced perturbations are not negligible.

[66] M. Celio, New method to calculate the muon polarization function, Phys. Rev. Lett. **56**, 2720 (1986).

[67] P. Bonfà, J. Frassineti, M. M. Isah, I. J. Onuorah, and S. Sanna, UNDI: An open-source library to simulate muon-nuclear interactions in solids, Comput. Phys. Commun. **260**, 107719 (2021).

[68] The value of the quadrupole moment of ^{51}V isotope is subject to a large uncertainty. The estimate used throghout the manuscript has been taken from Refs. [83,84], but in the same document, values differing by more than 25% are reported. In the literature, a value of $Q = -0.05$ barn is also commonly adopted [85], and we note that this would further improve the agreement between our first-principles simulations and the experimental results.

[69] This is trivially the result of the larger dipolar contribution of the closest Sb nucleus with respect to the more distant V nuclei.

[70] On the scale relevant for the present μSR experiment, the transition can be perfectly observed with, for example, ^{51}V NMR, which is sensitive to both EFGs and Knight shift variations. See, for example, Refs. [19,21].

[71] This value is computed by considering the half width at half maximum of a Lorentzian distribution. A similar conclusion is also reached by considering the variation of the Δ parameter.

[72] Q. Zhang, Y. Zhang, T. Wang, Z. Zhao, L. Zhou, B. Hou, H. Ji, H. Yang, T. Zhang, J.-T. Sun, H. Yang, H.-J. Gao, and Y. Wang, Temperature-driven rotation symmetry-breaking states in an atomic kagome metal KV_3Sb_5, Nano Lett. **24**, 6560 (2024).

[73] F. Grandi, A. Consiglio, M. A. Sentef, R. Thomale, and D. M. Kennes, Theory of nematic charge orders in kagome metals, Phys. Rev. B **107**, 155131 (2023).

[74] N. P. Bentley and S. J. Blundell, The interaction between a positive muon and multiple quadrupolar nuclei, J. Phys.: Conf. Ser. **2462**, 012043 (2023).

[75] A. Dal Corso, Pseudopotentials periodic table: From H to Pu, Comput. Mater. Sci. **95**, 337 (2014).

[76] J. P. Perdew, A. Ruzsinszky, G. I. Csonka, O. A. Vydrov, G. E. Scuseria, L. A. Constantin, X. Zhou, and K. Burke, Restoring the density-gradient expansion for exchange in solids and surfaces, Phys. Rev. Lett. **100**, 136406 (2008).

[77] H. J. Monkhorst and J. D. Pack, Special points for Brillouin-zone integrations, Phys. Rev. B **13**, 5188 (1976).

[78] D. Ceresoli, A. P. Seitsonen, U. Gerstmann, E. Kucukbenli, S. de Gironcoli, P. Giannozzi, N. Varini, M. Calandra, L. Paulatto, C. Cavazzoni, A. D. Corso, F. Spiga, and A. Ferreira, QE-GIPAW (2024), https://github.com/dceresoli/qe-gipaw.

[79] P. Giannozzi, S. Baroni, N. Bonini, M. Calandra, R. Car, C. Cavazzoni, D. Ceresoli, G. L. Chiarotti, M. Cococcioni, I. Dabo, A. Dal Corso, S. de Gironcoli, S. Fabris, G. Fratesi, R. Gebauer, U. Gerstmann, C. Gougoussis, A. Kokalj, M. Lazzeri, and L. Martin-Samos *et al.*, QUANTUM ESPRESSO: a modular and open-source software project for quantum simulations of materials, J. Phys.: Condens. Matter **21**, 395502 (2009).

[80] P. Giannozzi, O. Andreussi, T. Brumme, O. Bunau, M. B. Nardelli, M. Calandra, R. Car, C. Cavazzoni, D. Ceresoli, M. Cococcioni, N. Colonna, I. Carnimeo, A. D. Corso, S. de Gironcoli, P. Delugas, R. A. DiStasio, Jr., A. Ferretti, A. Floris, G. Fratesi, and G. Fugallo *et al.*, Advanced capabilities for materials modelling with QUANTUM ESPRESSO, J. Phys.: Condens. Matter **29**, 465901 (2017).

[81] I. Carnimeo, F. Affinito, S. Baroni, O. Baseggio, L. Bellentani, R. Bertossa, P. D. Delugas, F. F. Ruffino, S. Orlandini, F. Spiga, and P. Giannozzi, QUANTUM ESPRESSO: One further step toward the exascale, J. Chem. Theory Comput. **19**, 6992 (2023).

[82] A. Abragam, Spectrométrie par croisements de niveaux en physique du muon, Compt. Rend. Acad. Sci. Ser. II **299**, 95 (1984).

[83] N. J. Stone, Table of nuclear electric quadrupole moments, At. Data Nucl. Data Tables **111–112**, 1 (2016).

[84] T. J. Mertzimekis, Nuclear elecromagnetic moments, 2014, https://www-nds.iaea.org/nuclearmoments/isotope_measurement_results.php?A=51&Z=23.

[85] R. A. Bennett and H. O. Hooper, Magnitude of the ^{51}V nuclear electric quadrupole moment, J. Chem. Phys. **52**, 5485 (1970).

[86] P. Bonfà, I. J. Onuorah, P. Baker, Z. Guguchia, D. Valenti, S. Wilson, R. De Renzi, S. Sanna, N. Desportes De La Fosse, and G. Zotti, Follow the charge: Orbital reorganization across the time-reversal symmetry breaking transition in kagome superconductors (ISIS Facility, 2024), https://doi.org/10.5286/ISIS.E.RB2410449.